AN EFFICIENT SECOND-ORDER ACCURATE SHOCK-CAPTURING SCHEME FOR MODELING ONE AND TWO-PHASE WATER HAMMER FLOWS

Arturo S. León[1], Mohamed S. Ghidaoui, M. ASCE[2],

Arthur R. Schmidt, M. ASCE[3], Marcelo H. García, M. ASCE[4]

Abstract

This paper focuses on the formulation and assessment of a second-order accurate Finite Volume (FV) shock-capturing scheme for simulating one and two-phase water hammer flows. The two-phase flow model is based on the single-equivalent fluid concept. The proposed scheme for one and two-phase flows is the same, except the Riemann solvers used

[1]Ph.D. Candidate, Dept. of Civil and Environmental Eng., University of Illinois at Urbana-Champaign, Urbana, Illinois 61801, USA. Phone: (217)333-6178; Fax: (217)333-0687; E-mail: asleon@uiuc.edu (corresponding author)

[2]Professor, Dept. of Civil Engineering, The Hong Kong University of Science and Technology, Hong Kong. Phone: (852)2358-7174; Fax: (852)2358-1534; E-mail: ghidaoui@ust.hk

[3]Research Assistant Professor, V.T. Chow Hydrosystems Lab., Dept. of Civil and Envir. Eng., University of Illinois at Urbana-Champaign, Urbana, IL 61801, USA. Phone: (217)333-4934; Fax: (217)333-0687; E-mail: aschmidt@uiuc.edu

[4]Chester and Helen Siess Professor and Director, V.T. Chow Hydrosystems Lab., Dept. of Civil and Envir. Eng., University of Illinois at Urbana-Champaign, Urbana, IL 61801, USA. Phone: (217)244-4484; Fax: (217)333-0687; E-mail: mhgarcia@uiuc.edu

to evaluate fluxes between computational cells. For one-phase flows, the accuracy and numerical efficiency of the proposed scheme is contrasted against the fixed-grid Method of Characteristics (MOC) and a recently proposed FV scheme. For two-phase flows, the accuracy and numerical efficiency of the proposed scheme is compared to the fixed-grid MOC scheme. The results for one-phase flows show that, when a Courant number (Cr) very close to 1.0 (around 0.99 or higher) is used, the MOC scheme is more efficient than the proposed scheme and the other FV scheme. In this case, the latter two schemes have similar numerical efficiency. When Cr drops below about 0.95, the proposed scheme is more efficient than the MOC scheme and the other FV scheme, especially for smooth transient flows (no discontinuities). For two-phase water hammer flows, all the simulations were carried out using a maximum Courant number of 0.95 to avoid numerical instability problems. The results for two-phase flows show that the proposed scheme is much more efficient than the fixed-grid MOC scheme. The fixed-grid MOC and the proposed scheme are also used to reproduce a set of two-phase flow experiments reported in the literature. Good agreement between simulated and experimental data is found.

Keywords: Pressurized flow; Real-time control; Transients; Two-phase flow; Water hammer.

Introduction

The study of one and two-phase water hammer flows has great significance in a wide range of industrial and municipal applications including power plants, petroleum industries, water distribution systems, sewage pipelines, etc. For Real-Time Control (RTC) of these systems, the numerical efficiency of transient flow models is a critical factor, since several simulations are required within a control loop in order to optimize the control strategy, and small

simulation time steps are needed to reproduce the rapidly varying hydraulics (e.g., León et al. 2005, León et al. 2006). RTC is becoming increasingly indispensable for industrial and municipal applications in general. For instance, in the case of water distribution systems, RTC facilitates delivery of safe, clean and high-quality water in the most expedient and economical manner. Current methods available for modeling one and two-phase water hammer flows are briefly described next.

Methods for one-phase water hammer flows

Among the approaches proposed to solve the one-phase (pure liquid) water hammer equations are the Method of Characteristics (MOC), Finite Differences (FD), Wave Characteristic Method (WCM), Finite Elements (FE), and Finite Volume (FV). In-depth discussions of these methods can be found in Chaudhry and Hussaini 1985, Ghidaoui and Karney 1994, Szymkiewicz and Mitosek 2004, Zhao and Ghidaoui 2004, and Wood et al. 2005. Among these methods, MOC-based schemes are most popular because these schemes provide the desirable attributes of accuracy, numerical efficiency and programming simplicity (e.g., Wylie and Streeter 1983, Zhao and Ghidaoui 2004, Ghidaoui et al. 2005). In fact, in a review of commercially available water hammer software packages, it is found that eleven out of fourteen software packages examined use MOC schemes (Ghidaoui et al. 2005).

Recently, FV Godunov-Type Schemes (GTS) that belong to the family of shock-capturing schemes have been applied to one-phase water hammer problems with good success. The underlying idea of GTS is the Riemann problem that must be solved to provide fluxes between computational cells. The first application of GTS to one-phase water hammer problems is due to Guinot (2000), who presented first and second-order schemes based on Taylor series expansions of the Riemann invariants. He showed that his

second-order scheme is largely superior to his first-order scheme, although the Taylor series development introduces inaccuracies in the estimated pressure, especially in the case of low pressure-wave celerities. A second application is due to Hwang and Chung (2002), whose second-order accuracy scheme is based on the conservative form of the compressible flow equations. Although this scheme requires an iterative process to solve the Riemann problem, these authors state that their scheme requires a little more arithmetic operation and CPU time than the so-called Roe's scheme, but is able to get more accurate computational results than the latter scheme. Later, Zhao and Ghidaoui (2004) presented first and second-order schemes for solution of the non-conservative water hammer equations. These authors show that, for a given level of accuracy, their second-order GTS requires much less memory storage and execution time than either their first-order GTS or the fixed-grid MOC scheme with space-line interpolation. It is pointed out that the numerical tests carried out by these authors were for low Courant numbers. When a Courant number very close to 1.0 (around 0.99 or higher) is used, as shown in the present paper, the MOC scheme can be more efficient than the scheme of Zhao and Ghidaoui.

Methods for two-phase water hammer flows (single-equivalent fluid approximation)

The partial differential equations that describe two-phase flows in closed conduits can be simplified to a great extent when the amount of gas in the conduit is small. In this case, the gas-liquid mixture can be treated as a single-equivalent fluid (e.g., Wylie and Streeter 1983, Chaudhry et al. 1990, Martin 1993, Guinot 2001a). The governing equations when using the single-equivalent fluid approximation are identical to those for a one-phase flow. Due to this fact, similar techniques to those for a one-phase flow are used to solve the

two-phase flow governing equations that are based on the single-equivalent fluid concept. However, since shocks may be produced during transient conditions in two-phase flows (e.g., Padmanabhan and Martin 1978), only those methods that can handle shocks without special treatment are suitable for these applications.

In the literature, numerical schemes that have been proposed for modeling one-dimensional two-phase flows using the single-equivalent fluid approximation include MOC schemes, Lax-Wendroff schemes, a plethora of explicit schemes, and implicit methods (e.g., Chaudhry et al. 1990, Martin 1993). The MOC scheme requires isolation of shocks. The Lax-Wendroff scheme has the advantage that shock waves can be handled without special treatment (e.g., Martin 1993). However, the solution produces an overshooting of the shock front, followed by damped oscillations. These oscillations can be eliminated by introducing pseudo-viscosity. Artificial damping may be also necessary when using explicit schemes (e.g., Martin 1993). When using implicit methods, biasing or weighting problems may be encountered (e.g., Martin 1993). Recently, Guinot (2001a, 2001b) has applied GTS schemes to two-phase flows with good success. The first-order GTS presented by Guinot (2001a) showed that numerical diffusion leads to a very fast degradation of the solution quality after a few oscillation periods. The second-order scheme by Guinot (2001b) is largely superior to his first-order scheme, although an iterative process is required to solve the Riemann problem.

The present paper focuses on the formulation and numerical efficiency assessment of a second-order accurate FV shock-capturing scheme for simulating one and two-phase water hammer flows. In the proposed approach, no iteration is required for the solution of the Riemann problem for both types of flow. This paper is organized as follows: (1) the governing

equations are presented in conservation-law form; (2) the corresponding FV discretization is described; (3) a brief description of the proposed second-order scheme for the internal cells is presented; (4) Riemann solvers for the flux computation at the cell interfaces are provided; (5) a brief description for the formulation of second-order boundary conditions is presented; (6) stability constraints are provided; and (7) results from testing the proposed model under one and two-phase flow conditions are presented.

Governing Equations

The governing equations that describe two-phase flows in closed conduits can be simplified to a great extent when the amount of gas in the conduit is small. In this case, it can be assumed that there is no relative motion or slip between the gas and the liquid and both phases can be treated as a "single-equivalent fluid" with average properties (e.g., Martin 1993, Wylie and Streeter 1983). Furthermore, the characteristic time scale of the transients is so small that adsorption/desorption of gas can be considered negligibly small (Zielke et al. 1989). The mass and momentum conservation equations for the "single-equivalent fluid" assumptions are identical to those for a liquid-phase flow and can be written in their vector conservative form as follows (e.g., Chaudhry 1987, Martin 1993):

$$\frac{\partial \mathbf{U}}{\partial t} + \frac{\partial \mathbf{F}}{\partial x} = \mathbf{S} \tag{1}$$

where the vector variable $\mathbf{U}$, the flux vector $\mathbf{F}$ and the source term vector $\mathbf{S}$ may be written as:

$$\mathbf{U} = \begin{bmatrix} \Omega \\ Q_m \end{bmatrix}, \mathbf{F} = \begin{bmatrix} Q_m \\ \frac{Q_m^2}{\Omega} + A_f p \end{bmatrix} \text{ and } \mathbf{S} = \begin{bmatrix} 0 \\ (S_0 - S_f)\rho_f g A_f \end{bmatrix} \tag{2}$$

where ρ_f is the fluid density, A_f is the full cross-sectional area of the conduit, $\Omega = \rho_f A_f$ is the mass of fluid per unit length of conduit, $Q_m = \Omega u$ is the mass discharge, u is the

water velocity, p is the pressure acting on the center of gravity of A_f, g is the gravitational acceleration, S_0 is the slope of the conduit, and S_f is the slope of the energy line.

The vector Eq. 1 does not form a closed system in that the flow state is described using three variables: Ω, p and Q_m. However, it is possible to eliminate the pressure variable by introducing the general definition of the celerity of the pressure wave (a_g) [e.g., Guinot 2003], which relates p and Ω:

$$a_g = \left[\frac{d(A_f p)}{d\Omega}\right]^{1/2} \tag{3}$$

The pressure-wave celerity for the gas-liquid mixture (a_m) can be estimated as (Guinot 2001a):

$$a_m = \frac{a}{\sqrt{1 + \psi_{ref}\rho_{f\,ref}a^2 \frac{p_{ref}^{\frac{1}{\beta}}}{p^{\frac{1+\beta}{\beta}}}}} \tag{4}$$

where a is the pressure-wave celerity in presence of liquid only, p_{ref} is a reference pressure for which the density is known ($\rho_{f\,ref}$), β is a coefficient equal to 1.0 for isothermal processes and 1.4 for adiabatic conditions, and ψ_{ref} is the volume fraction of gas at the reference pressure. The water density measured at a temperature of 4 degrees Celsius under atmospheric pressure conditions is 1000 kg/m^3. Thus, the reference density and pressure when the liquid is water can be taken as 1000 kg/m^3 and 101325 Pa, respectively.

The relationship between the volume fraction of gas ψ and pressure for the "single-equivalent fluid" assumptions can be expressed as (e.g., Guinot 2001a):

$$p\psi^{\beta} = p_{ref}\psi_{ref}^{\beta} \tag{5}$$

The pressure-wave celerity in presence of liquid only depends upon the elastic properties of the conduit, the bulk modulus of elasticity of the fluid, as well as on the external constraints.

The general expression of the pressure-wave celerity is given by (e.g., Chaudhry 1987):

$$a = \left[\frac{k_f/\rho_f}{1 + \frac{k_f}{Y}\chi} \right]^{1/2} \tag{6}$$

where k_f is the bulk modulus of elasticity of the fluid, Y is Young's modulus of elasticity of the pipe material, and χ is a non-dimensional parameter that depends upon the geometric properties of the conduit and pipe restraints. Substituting Eq. 4 into Eq. 3 and integrating the differentials $d\Omega$ and dp (A_f is assumed to be constant) leads to the following equation that relates p and Ω:

$$\Omega = \Omega_{ref} + \frac{A_f}{a^2}\left[p - p_{ref} + (p_{ref}^{\frac{-1}{\beta}} - p^{\frac{-1}{\beta}})\beta\psi_{ref}\rho_{f\,ref}a^2 p_{ref}^{\frac{1}{\beta}} \right] \tag{7}$$

where $\Omega_{ref} = \rho_{f\,ref}A_f$. The pressure p in Eq. 7 can be determined by an iterative scheme such as the Newton Raphson method and typically between three and five iterations are needed to ensure convergence. In one-phase liquid flows, the pressure-wave celerity is constant and no iteration is required to determine p. In this case, the following relation between p and Ω is obtained:

$$p = p_{ref} + \frac{a^2}{A_f}(\Omega - \Omega_{ref}) \tag{8}$$

The flow variables used in this paper are Ω and Q_m. However, the engineering community prefers to use the piezometric head h and flow discharge Q. The latter variables can be determined from Ω and Q_m as follows:

$$Q = \frac{Q_m}{\Omega}A_f \tag{9}$$

$$h = \frac{p - p_{ref}}{\rho_{f\,ref}g} + \frac{d}{2} \tag{10}$$

where d is the pipe diameter and h is measured over the conduit bottom. The absolute pressure head (H) in meters of water can be obtained as $H = h + 10.33$.

Formulation of Finite Volume Godunov-type schemes

This method is based on writing the governing equations in integral form over an elementary control volume or cell, hence the general term of Finite Volume (FV) method. The computational grid or cell involves discretization of the spatial domain x into cells of length Δx_i and the temporal domain t into intervals of duration Δt. The ith cell is centered at node i and extends from $i-1/2$ to $i+1/2$. The flow variables (Ω and Q_m) are defined at the cell centers i and represent their average value within each cell. Fluxes, on the other hand are evaluated at the interfaces between cells ($i-1/2$ and $i+1/2$). For the ith cell, the updating FV formula for the left side of Eq. (1) is given by (e.g., Toro 2001, LeVeque 2002)

$$\mathbf{U}_i^{n+1} = \mathbf{U}_i^n - \frac{\Delta t}{\Delta x_i}(\mathbf{F}_{i+1/2}^{n+1/2} - \mathbf{F}_{i-1/2}^{n+1/2}) \tag{11}$$

where the superscripts n, $n+1/2$, and $n+1$ reflect the t, $t+\Delta t/2$, and $t+\Delta t$ time levels, respectively. To introduce the source terms (right side of Eq. 1) into the solution, a time splitting method using a second-order Runge-Kutta discretization is used (e.g., Zhao and Ghidaoui 2004, León et al. 2006). In the Godunov approach, the flux $\mathbf{F}_{i+1/2}^{n+1/2}$ is obtained by solving the Riemann problem with constant states $\mathbf{U}_i^n$ and $\mathbf{U}_{i+1}^n$. This way of computing the flux leads to a first-order accuracy of the numerical solution. To achieve second-order accuracy in space and time, the Monotone Upstream-centred Scheme for Conservation Laws (MUSCL)-Hancock method is used in this paper, which is described in the next section.

The MUSCL-Hancock method

The first step of the MUSCL-Hancock method (e.g., Toro 2001) is the reconstruction of piece-wise constant data $\mathbf{U}_i^n$ into a piecewise linear distribution of the data $\big($e.g., $\mathbf{U}_i^n(x) =$

$\mathbf{U}_i^n + (x - x_i)\Delta i/\Delta x$, where $x_i = (i - 1/2)\Delta x$ is the center of the computing cells and Δi is a vector difference $[\Delta i = (\mathbf{U}_{i+1}^n - \mathbf{U}_{i-1}^n)/2]\big)$, and then extrapolation of the data to the edges of each cell, yielding the extrapolated values $\mathbf{U}_L$ and $\mathbf{U}_R$. To avoid spurious oscillations near shock waves and other sharp flow features, a Total Variation Diminishing (TVD) constraint is enforced in the data reconstruction step by limiting Δ_i. The MINMOD pre-processing slope limiter is used in this paper to enforce the TVD constraint. This limiter is found to be the most stable especially in two-phase flows conditions when Courant numbers very close to 1.0 are used. The reader is referred to Toro (2001) for a detailed description of the available limiters.

The second step consists in evolving the extrapolated values through a half time step according to

$$\widetilde{\mathbf{U}}_{L,R} = \mathbf{U}_{L,R} - \frac{1}{2}\frac{\Delta t}{\Delta x}\Big[\mathbf{F}(\mathbf{U}_R) - \mathbf{F}(\mathbf{U}_L)\Big]. \tag{12}$$

where $\mathbf{F}(\mathbf{U})$ indicates the flux of $\mathbf{U}$.

In the third step, a Riemann problem with initial data consisting of evolved boundary extrapolated values is solved. In what follows, approximate Riemann solvers for one and two-phase water hammer flows that do not require iterations are proposed.

Riemann solver for one-phase water hammer flows

In this type of flows, the pressure-wave celerity is constant and the order of magnitude of u is much smaller than a, so the convective term in the governing equations can be neglected. Since u is much smaller than a_m, the characteristics travel in opposite directions and the star region ($\star$), which is an intermediate region between the left and right states, contains the location of the initial discontinuity. Hence, the flow variables in the star region

are used to compute the flux. The solution of the Riemann problem for the linearized hyperbolic system $\partial \mathbf{U}/\partial t + \overline{\mathbf{A}}\partial \mathbf{U}/\partial x = 0$ provides the following estimates for $\Omega_\star$ and $Qm_\star$ (The derivation details of $\Omega_\star$ and $Qm_\star$ for one-phase water hammer flows are similar to those for two-phase water hammer flows. Due to space limitations, only the derivation details of $\Omega_\star$ and $Qm_\star$ for two-phase water hammer flows are presented in Appendix A)

$$\Omega_\star = \frac{\Omega_L + \Omega_R}{2} + \frac{Qm_L - Qm_R}{2a} \tag{13}$$

$$Qm_\star = \frac{Qm_L + Qm_R}{2} + a\frac{\Omega_L - \Omega_R}{2} \tag{14}$$

which are used to compute the flux by using Eq. 2.

Riemann solver for two-phase water hammer flows

In contrast with one-phase water hammer flows, in two-phase flows the pressure-wave celerity may be reduced to very low values, in which case u is not necessarily negligible compared to a_m. However, u is still smaller than a_m and consequently the characteristics travel in opposite directions and the star region contains the location of the initial discontinuity. Hence, the flow variables in the star region are used to compute the flux. Simple estimates for $\Omega_\star$ and $Qm_\star$ that do not require iterations can be obtained by solving the Riemann problem for the linearized hyperbolic system $\partial \mathbf{U}/\partial t + \overline{\mathbf{A}}\partial \mathbf{U}/\partial x = 0$ that yields (see Appendix A for derivation details):

$$\Omega_\star = \left(\frac{\Omega_L + \Omega_R}{2}\right)\left(1 + \frac{u_L - u_R}{2\bar{a}_m}\right) \tag{15}$$

$$Qm_\star = Qm_L + (\bar{u} - \bar{a}_m)\left(\Omega_\star - \Omega_L\right) \tag{16}$$

where $\bar{a}_m = (a_{m_L} + a_{m_R})/2$ and $\bar{u} = (u_L + u_R)/2$. By using the estimated values of $\Omega_\star$ and $Qm_\star$, the flux is obtained from Eq. 2.

Second-order accurate boundary conditions

Since Eq. 11 is to be used for all the cells of the computational domain, it is necessary to compute the fluxes $\mathbf{F}_{1/2}^{n+1/2}$ (left-hand boundary) and $\mathbf{F}_{Nx+1/2}^{n+1/2}$ (right-hand boundary) in order to update the flow variables in the first and last cells. For the quality of the numerical solution to be preserved, it is necessary to use the same order of reconstruction in all the cells of the computational domain (e.g., LeVeque 2002, Guinot 2003). The MUSCL-Hancock scheme uses one cell on each side of the cell in which the profile is to be reconstructed. Therefore, one cell is missing when the profile is to be reconstructed within the first and last cells of the computational domain. The missing information at the boundaries is restored by adding one virtual cell at each end of the computational domain. The virtual cell on the left-hand side is numbered 0, while the cell on the right-hand side of the domain is numbered $Nx+1$ (Fig. 1). The algorithm consists of the following steps: (1) determination of the flow variables at the boundaries $1/2$ and $Nx+1/2$, and (2) determination of the flow variables in the virtual cells.

Determination of the flow variables at the boundaries

It is assumed that the average flow variables in the cells 0 to $Nx+1$ are known from the previous time step and that a second-order reconstruction has been carried out in the cells 1 and Nx (Fig. 1). The unknown boundary flow variables ($\mathbf{U}_b$) are determined using the theory of Riemann invariants. The reader is referred to the book of Leveque (2002) for a deeper discussion on the theory of Riemann invariants. The generalized Riemann invariants for two-phase water hammer flows are given by (e.g., Guinot 2003):

$$\begin{cases} (a_m/\Omega)d\Omega + du = 0 \ \text{ along } dx/dt = u + a_m \\ (a_m/\Omega)d\Omega - du = 0 \ \text{ along } dx/dt = u - a_m \end{cases} \tag{17}$$

Due to space limitations, only the procedure to compute the flux at the left-hand boundary is provided in this section. However, the algorithm is very similar for the right-hand boundary. The left-hand boundary (b) is connected to the left of the first cell $(1,L)$ along the characteristic $dx/dt = u - a_m$ (Fig. 2). Thus, for the left-hand boundary, the second relationship of Eq. 17 is integrated between b and $(1,L)$, which integration can be approximated according to the trapezoidal rule as follows:

$$\frac{a^n_{m1,L} + a^{n+1/2}_{m_b}}{2}(\Omega^{n+1/2}_b - \Omega^n_{1,L}) - \frac{\Omega^n_{1,L} + \Omega^{n+1/2}_b}{2}(u^{n+1/2}_b - u^n_{1,L}) = 0 \tag{18}$$

Another relationship is available from prescribing one flow variable or an equation that relates the two flow variables at the boundary. This relationship (ζ_b) may be expressed as:

$$\zeta_b(\Omega^{n+1/2}_b, Q^{n+1/2}_{m_b}) = 0 \tag{19}$$

Depending on the type of boundary condition imposed, it may or may not be necessary to use an iterative technique to solve the system of Eqs. 18 and 19. Determined the flow variables at the boundaries ($\mathbf{U}^{n+1/2}_b$), the boundary fluxes can be computed by using the flux relation in Eq. 2.

For instance, let's consider that the pressure is prescribed at the left-hand boundary ($p^{n+1/2}_b$). This is equivalent to prescribing a mass per unit length $\Omega^{n+1/2}_b$, computed from Eq. 7.

$$\Omega_b = \Omega_{ref} + \frac{A_f}{a^2}\left[p_b - p_{ref} + (p_{ref}^{\frac{-1}{\beta}} - p_b^{\frac{-1}{\beta}})\beta\,\psi_{ref}\rho_{f\,ref}a^2 p_{ref}^{\frac{1}{\beta}}\right] \tag{20}$$

The value of $u_b^{n+1/2}$ is obtained from Eq. 18. This yields:

$$u_b^{n+1/2} = u_{1,L}^n + \frac{(a_{m_{1,L}}^n + a_{m_b}^{n+1/2})(\Omega_b^{n+1/2} - \Omega_{1,L}^n)}{\Omega_b^{n+1/2} + \Omega_{1,L}^n} \tag{21}$$

Since the pressure is prescribed at the boundary, $a_{m_b}^{n+1/2}$ is known from Eq. 4. Thus $u_b^{n+1/2}$ is the only unknown in Eq. 21. Once $u_b^{n+1/2}$ is determined, $Q_{m_b}^{n+1/2}$ can be calculated ($Q_{m_b}^{n+1/2} = \Omega_b^{n+1/2} u_b^{n+1/2}$). Once $\Omega_b^{n+1/2}$, $Q_{m_b}^{n+1/2}$, and $A_f p_b^{n+1/2}$ are known, the flux at the left-hand boundary $\mathbf{F}_b^{n+1/2} = \mathbf{F}_{1/2}^{n+1/2}$ can be computed by using the flux relation in Eq. 2.

Now, let's consider that the discharge is prescribed at the left-hand boundary ($Q_b^{n+1/2}$). Prescribing $Q_b^{n+1/2}$ is equivalent to prescribing a velocity $u_b^{n+1/2} = Q_b^{n+1/2}/A_f$. Eq. 18 can be solved for $\Omega_b^{n+1/2}$ as

$$\Omega_b^{n+1/2} = \left[1 + 2\frac{u_b^{n+1/2} - u_{1,L}^n}{a_{m_{1,L}}^n + a_{m_b}^{n+1/2} - u_b^{n+1/2} + u_{1,L}^n}\right]\Omega_{1,L}^n \tag{22}$$

in which $\Omega_b^{n+1/2}$ and $a_{m_b}^{n+1/2}$ are the unknowns. The solution is found iteratively. A first guess is made for $\Omega_b^{n+1/2}$ (for instance $\Omega_b^{n+1/2} = \Omega_{1,L}^n$) and this first guess is inserted into Eq. 20 to compute $p_b^{n+1/2}$. The computed value of $p_b^{n+1/2}$ in turn is inserted into Eq. 4 to compute $a_{m_b}^{n+1/2}$. This value is used in Eq. 22 to update $\Omega_b^{n+1/2}$, the new value of which is used to compute $a_{m_b}^{n+1/2}$. The procedure is repeated until convergence is achieved. Once $\Omega_b^{n+1/2}$ is determined, $p_b^{n+1/2}$ can be calculated from Eq. 20. Once $\Omega_b^{n+1/2}$, $A_f p_b^{n+1/2}$, and $Q_{m_b}^{n+1/2} (= \Omega_b^{n+1/2} u_b^{n+1/2})$ are known, $\mathbf{F}_{1/2}^{n+1/2}$ can be computed as in the previous case.

For one-phase flows, the fluxes at the boundaries can be also obtained from the generalized Riemann invariants. Since in one-phase water hammer flows the flow velocity is much smaller than the pressure-wave celerity, the convective term (Q_m^2/Ω) in the flux vector in Eq. 2 is neglected. In this case, if a pressure is prescribed at the left-hand boundary

($p_b^{n+1/2}$), the following relations are obtained for $\Omega_b^{n+1/2}$ and $Q_{m_b}^{n+1/2}$:

$$\Omega_b^{n+1/2} = \Omega_{ref} + \frac{A_f}{a^2}(p_b^{n+1/2} - p_{ref}) \tag{23}$$

$$Q_{m_b}^{n+1/2} = Q_{m_{1,L}}^{n} + a(\Omega_b^{n+1/2} - \Omega_{1,L}^{n}) \tag{24}$$

Because the convective term was neglected, only $A_f p_b^{n+1/2}$, and $Q_{m_b}^{n+1/2}$, are substituted into the flux vector $\mathbf{F}_{1/2}^{n+1/2}$ in Eq. 2.

Likewise, if a discharge is prescribed at the left-hand boundary ($Q_b^{n+1/2}$), the following relations are obtained for $\Omega_b^{n+1/2}$ and $Q_{m_b}^{n+1/2}$:

$$\Omega_b^{n+1/2} = \frac{Q_{m_{1,L}}^{n} - a\Omega_{1,L}^{n}}{Q_b^{n+1/2}/A_f - a} \tag{25}$$

$$Q_{m_b}^{n+1/2} = \frac{Q_b^{n+1/2}}{A_f}\Omega_b^{n+1/2} \tag{26}$$

The value of $\Omega_b^{n+1/2}$ can be substituted in Eq. 8 to determine $p_b^{n+1/2}$. Once $A_f p_b^{n+1/2}$, and $Q_{m_b}^{n+1/2}$ are known, $\mathbf{F}_{1/2}^{n+1/2}$ can be computed as in the previous case.

Determination of the flow variables in the virtual cells

Virtual cells are used only to achieve second-order accuracy in the first and last cells of the computational domain. Therefore, they should advect the same outflowing information as that at the boundaries and they should maintain the conservation property of the shock capturing scheme. The latter means that no unphysical perturbations into the computational domain may be introduced by the virtual cells. These constraints may be satisfied: (1) by assuming that the outflowing wave strengths in the virtual cells are the same as those at the boundaries, and (2) by adjusting the inflowing wave strengths in the virtual cells in such a way that the fluxes in these cells are the same as those at the respective boundaries. For the

left hand boundary, a simple formulation that satisfies these two conditions is given by:

$$\begin{aligned} \Omega_0^{n+1} &= \Omega_{1/2}^{n+1/2} = \Omega_b^{n+1/2} \\ Q_{m_0}^{n+1} &= Q_{m_{1/2}}^{n+1/2} = Q_{m_b}^{n+1/2} \end{aligned} \tag{27}$$

Note in Eq. 27 that the flow variables at the left-hand boundary ($\mathbf{U}_{1/2}^{n+1/2}$) at time level "$n+1/2$" are adopted by the virtual cell "0" at time level "$n+1$". The flow variables in the virtual cell "0" at time level "$n+1$" are used for the reconstruction of the flow variables in cell "1" at this time level, unless monotonicity needs to be preserved in this cell.

Stability constraints

In a similar way to Zhao and Ghidaoui (2004), in this paper the source terms $\mathbf{S}$ are introduced into the solution through time splitting using a second-order Runge-Kutta discretization. Since this discretization is explicit, the stability constraint must include not only the Courant-Friedrichs-Lewy (CFL) criterion for the convective part, but also the constraint for the source terms. The CFL constraint is given by:

$$\Delta t_{\text{max, CFL}} = \text{Min}_{\ i=1,2,...Nx} \left[\frac{\Delta x_i}{|u_i^n| + |a_{m_i}^n|} \right] \tag{28}$$

and the constraint due to the explicit second-order Runge-Kutta discretization is given by (León et al. 2006)

$$\Delta t_{max,\mathbf{S}} = \text{Min}_{\ i=1,2,...Nx} \left[-4 \frac{\mathbf{U}_i^{n+1}}{\mathbf{S}(\mathbf{U}_i^{n+1})}, -2 \frac{\mathbf{U}_i^{n+1}}{\mathbf{S}(\overline{\mathbf{U}}_i^{n+1})} \right] \tag{29}$$

where $\mathbf{S}(\mathbf{U})$ indicates that $\mathbf{U}$ is used to evaluate the source term $\mathbf{S}$. The evaluation of $\mathbf{S}$ requires the definition of the grid bottom slope $(S_0)_i$ given by

$$(S_0)_i = -\frac{z_{i+1/2} - z_{i-1/2}}{x_{i+1/2} - x_{i-1/2}} = -\frac{\Delta z_i}{\Delta x_i} \tag{30}$$

and the grid energy line slope $(S_f)_i$ which may be expressed as $(S_f)_i = f u_i |u_i| / (2gd)$, where f is the Darcy-Weisbach friction factor.

Since the same time step Δt must be used for the convective part and the source term, $\mathbf{U}_i^n$ must be used instead of $\mathbf{U}_i^{n+1}$. Finally, the maximum permissible time step including the convective part and the source term will be given by:

$$\Delta t_{max} = \text{Min}_{\ i=1,2,...Nx}\left[\Delta t_{max,\mathbf{S}},\ \Delta t_{\text{max, CFL}}\right] \tag{31}$$

Evaluation of the model

The purpose of this section is to asses the accuracy and numerical efficiency of the proposed scheme for modeling one and two-phase water hammer flows. For one-phase flows, the accuracy and numerical efficiency of the proposed scheme is compared against those of the fixed-grid MOC scheme with space-line interpolation and the second-order scheme of Zhao and Ghidaoui (ZG). For two phase flows, the accuracy and numerical efficiency of the proposed scheme is compared against that of the fixed-grid MOC scheme with space-line interpolation. The proposed approach and the MOC scheme are also used to reproduce a set of two-phase flow experiments reported in the literature. Four tests cases are considered in this section. These are:

(1) Instantaneous downstream valve closure in a frictionless horizontal pipe (one-phase flow)

(2) Gradual downstream valve closure in a frictionless horizontal pipe (one-phase flow)

(3) Instantaneous downstream valve closure in a frictionless horizontal pipe (two-phase flow)

(4) Comparison with two-phase flow experiments of Chaudhry et al. (1990)

The proposed approach is valid for pipes with and without friction. In the three first tests, frictionless pipes are used only because in such cases the physical dissipation is zero,

so any dissipation or amplification in the results is solely due to the numerical scheme. In the following sections, the number of grids, grid size and Courant number used in each example are indicated in the relevant figures and thus will not be repeated in the text. The CPU times that are reported in this paper were averaged over three realizations and computed using a HP AMD Athlon (tm) 64 processor 3200 + 997 MHz, 512 MB of Ram notebook.

Test 1: Instantaneous downstream valve closure in a frictionless horizontal pipe (one-phase flow)

This test is used to compare the accuracy and numerical efficiency of the proposed scheme against the Zhao and Ghidaoui (2004) approach and the MOC scheme with space-line interpolation for one-phase flows under strong transient conditions. As an aside, a strong transient refers to a transient phenomena in which the resulting flow presents discontinuities (sharp fronts). This type of transient is generated for instance after an instantaneous valve closure. On the other hand, a smooth transient refers to a transient phenomena in which the resulting flow doesn't present discontinuities. This transient is produced for instance after a gradual valve closure. The test considers one horizontal frictionless pipe connected to an upstream reservoir and a downstream valve. The length of the pipe is 10000 m and its diameter is 1.0 m, the pressure-wave celerity is 1000 m/s, the upstream reservoir constant head h_0 is 200 m, and the initial steady-state discharge is 2.0 m^3/s.

The transient flow is obtained after an instantaneous closure of the downstream valve. To investigate the performance of the schemes under consideration when using low Courant numbers, these schemes are used to reproduce the resulting transient using a coarse grid (to illustrate their performance better) and two low Courant numbers (Cr = 0.5 and Cr =

0.1). A portion of the simulated pressure traces are shown in Figs. 3(a) and 3(b). Additional simulations were performed using a $Cr = 1.0$. As expected, all schemes under consideration have reproduced the exact solution when $Cr = 1.0$ (results not shown). It is clear from Figs. 3(a) and 3(b) that the MOC is more dissipative than either the second-order scheme of Zhao and Ghidaoui or the proposed scheme for low Courant numbers. The results also show that the proposed scheme is less dissipative than the scheme of Zhao and Ghidaoui. The basic difference between the second-order scheme of Zhao and Ghidaoui and the proposed approach for one-phase flows is that only a first-order boundary condition is used in the former approach, and a second-order one in the latter.

In the previous simulations, the reader may question the low Courant numbers used. Although in real large-scale systems, whose pipes have different lengths and water hammer wavespeeds, it is impossible to achieve a Courant number of 1.0 when a coarse computational grid is chosen, it can be shown that by increasing the number of cells, a Cr close to 1.0 can be achieved. In the latter condition, a good performance of all schemes is expected. A realistic assessment of accuracy and numerical efficiency of the schemes has to take into account the variation of the Courant number with the number of grids (Nx). The variation of Cr versus Nx is not the same for different pipe systems. However, the trend of Cr vs Nx is similar for several scenarios tested (results not shown). The trend of Cr versus Nx adopted in this test case is presented in Fig. 4. This trend was obtained using the pipe system presented in Ghidaoui et al. (1998). This system consisted of two pipes in series where the length of the upstream pipe was 800 m and the length of the downstream one was 300 m. The pressure wave celerity for both pipes was 1000 m/s. The discretization strategy was based on the pipe that has the minimum wave travel time (Karney and Ghidaoui 1997).

The approach of using at least one reach in the pipe that has the minimum wave travel time guarantees that the Courant number in the remaining pipes of the system is bounded by 0.5 and 1.0.

To obtain a quantitative measure of numerical dissipation, the energy equation of Karney (1990) can be used (Ghidaoui et al. 1998). The energy equation of Karney states that the total energy (sum of internal and kinetic) can only change as work is done on the conduit or as energy is dissipated from it. In this test the friction is set to zero, so the rate of total energy dissipation is zero. Moreover, because the downstream valve is closed instantaneously, no fluid is exchanged with the environment across a pressure difference; therefore the work produced at the downstream end of the pipe is also equal to zero (Ghidaoui et al. 1998). As an aside, the rate of change of internal energy (δU) given in Karney (1990) in our notation is given by $\delta U = d[(\rho_f L A_f g^2 (h_s - h)^2)/(2a^2)]$, where h_s is the head after the transient flow has reached steady state measured over the conduit bottom. By integrating this relation considering that $U = 0$ at $h = h_s$, the expression for the internal energy at any time can be written as: $U = (\rho_f A_f g^2)/(2a^2) \int (h_s - h)^2 dx$. Notice in this test that h_s is the same as the head at the reservoir and thus, no work is produced at the reservoir. Therefore, the total energy (sum of kinetic and internal) in the pipe E is invariant with time (i.e., E/E_0 = 1.0).

Figure 5 shows relative energy traces E/E_0 produced by the schemes under consideration for two coarse grids (Nx = 10 and 20 cells). The Courant number associated to each number of cells is obtained from Fig. 4 (average trend) and its values are presented together with the number of cells in Fig. 5 caption. Fig. 5 shows that, the numerical dissipation produced by the proposed scheme using 10 cells is smaller than that obtained by either the

MOC scheme or the Zhao and Ghidaoui approach for the same number of cells. For instance, after 400 s, 29% of the initial energy has been dissipated by the MOC scheme, 21% by the scheme of Zhao and Ghidaoui and 18% by the proposed scheme. The numerical dissipation results for all the schemes produced using 20 cells show a significant reduction compared to those using 10 cells. This reduction is not only due to the increase of cell numbers (10 to 20) but mainly due to the associated increase of the Courant number (0.9829 to 0.9938). So far, it has been shown that, for coarse grids, the proposed scheme is more accurate than either the MOC scheme or the approach of Zhao and Ghidaoui. However, an objective comparison requires measuring the CPU time needed by each of the schemes to achieve the same level of accuracy (e.g., Zhao and Ghidaoui 2004, León et al. 2006).

To compare the numerical efficiency of the schemes, the numerical dissipation (numerical error) is plotted against the number of grids on log-log scale (Fig. 6). As shown in Fig. 6, for coarse grids, the accuracy of the proposed scheme is almost the same as Zhao and Ghidaoui and slightly superior than the MOC scheme. For relatively fine grids ($Nx >$ 1000), the accuracy of the three schemes is almost the same. For comparison of CPU times, five levels of numerical error were selected (0.1% - 10%). The number of grids needed by each scheme to achieve the five numerical error levels were obtained from Fig. 6. These number of grids in turn were used to determine their associated Courant numbers (Fig. 4) and the CPU times. Fig. 7 shows the plot of the numerical error against the CPU time on log-log scale. The CPU time results show that, to achieve the same degree of accuracy, the proposed scheme has a similar numerical efficiency as the Zhao and Ghidaoui scheme. The results also show that the MOC is more efficient numerically than the proposed scheme and the Zhao and Ghidaoui approach despite the fact that, for a given level of accuracy, the

MOC scheme requires a finer grid than the proposed scheme and the Zhao and Ghidaoui approach. For the CPU time results presented in Fig. 7, it is found that the MOC scheme is about 2 to 5 times faster to execute than the proposed scheme and the Zhao and Ghidaoui approach.

Test 2: Gradual downstream valve closure in a frictionless horizontal pipe (one-phase flow)

This test is used to compare the accuracy and numerical efficiency of the proposed scheme against the Zhao and Ghidaoui (2004) approach and the MOC scheme with space-line interpolation for one-phase flows under smooth transient conditions (no discontinuities). The test rig used is adapted from Wylie and Streeter (1983). This test rig considers one horizontal frictionless pipe connected to an upstream reservoir and a downstream valve. The length of the pipe is 600 m and its diameter is 0.5 m, the pressure-wave celerity is 1200 m/s, the upstream reservoir constant head h_0 is 150 m, and the initial steady-state discharge is 0.4882 m^3/s. The transient flow in this test is obtained after a gradual closure of the downstream valve. The valve closure relationship is given by $\tau = (1 - t/t_c)^{1.5}$ where t_c is the time of valve closure, which has been assumed to be 2.1 s.

In test 1 (strong transients), it was shown that when Cr is very close to 1.0 (around 0.99 or higher), the MOC scheme is more efficient than the proposed scheme and the Zhao and Ghidaoui approach. The same occurs in smooth (no discontinuities) transient conditions for one-phase flows. Due to space limitations, the results for smooth transient conditions are not shown. Courant number values of 0.99 and higher could potentially be achieved in single-phase and single-regime flows. In sewerage flows, however, Cr varies widely because (i) air entrapment and subsequent release and (ii) the interface between the pres-

surized part and the open channel part changes with time (i.e., the length of the water hammer column varies significantly in sewer surcharging problems.) Therefore, it is important that a scheme for transient flows in sewers remains efficient for a wide range of Cr values. In addition, for consistency, it is desired that a single scheme be used to model all various flow regimes. For open channel flows, which present a wide variation of Cr, it was found that FV schemes are much more efficient than the fixed-grid MOC scheme with space-line interpolation (León et al. 2006). The desire to use a single scheme for all flow regimes combined with the wide variation of Cr makes it important that any scheme adopted preserves both accuracy and efficiency throughout a wide range of Cr including small values.

Furthermore, even in single-phase and single-regime flows, as is shown in Fig. 4, although the Courant number trend approaches 1.0 when Nx is increased, the Courant number has a periodic variation with the number of grids. Thus, a Cr very close to 1.0 cannot be guaranteed in all the pipes. To investigate the performance of the schemes for Courant numbers slightly less than 1.0, a $Cr = 0.95$ is considered in this test. Fig. 8 shows simulated pressure traces at the downstream valve using this Courant number and $Nx = 40$ cells. The "Near exact" solution is also presented in this figure. The "Near exact" solution is obtained by grid refinement until convergence is achieved. As is shown in this figure, the MOC is more dissipative than either the second-order scheme of Zhao and Ghidaoui or the proposed scheme. The results also show that the proposed scheme is less dissipative than the scheme of Zhao and Ghidaoui.

To obtain a quantitative measure of numerical dissipation, the energy equation of Karney (1990) is also used here. In this test, work is produced at the downstream boundary while

fluid is exchanged with the environment across a pressure difference. Thus, the total energy (sum of kinetic and internal) is not invariant with time while the valve is being closed. After the valve is closed, no work is done or energy is dissipated on the conduit, and therefore the total energy is invariant with time. Figure 9 shows relative energy traces produced by the schemes under consideration for Cr = 0.95 and Nx = 40 cells. The relative energy is expressed as E/E_c, where E_c is the total energy after the valve is totally closed, and E is the total energy at time t. Figure 9 shows a reduction in the relative energy until the valve is totally closed ($t = 2.1s$). For $t > 2.1s$, the relative energy is constant and equal to 1.0. Since all numerical schemes are dissipative, the relative energy traces achieved by the schemes (after the valve is closed) are smaller than 1.0 (Fig. 9).

Fig. 10 shows the plot of the numerical error against the number of grids on log-log scale. As shown in this figure, to achieve a given level of accuracy, the MOC scheme requires a much finer grid than the proposed scheme and the Zhao and Ghidaoui approach. For comparison of CPU times, five levels of numerical error were selected (0.1% - 10%). The number of grids needed by each of the schemes to achieve the five levels of numerical error, were obtained from Fig. 10. These number of grids in turn were used to compute the CPU times. The numerical error is plotted as a function of the CPU time in Fig. 11. This figure shows that, to achieve the same degree of accuracy, the proposed scheme requires less CPU time than either the MOC scheme or the Zhao and Ghidaoui approach. For instance, for a numerical error of 1%, the CPU time required by the proposed scheme is about 0.04 and 0.71 times of those required by the MOC scheme and the Zhao and Ghidaoui approach, respectively. For the CPU time results presented in Fig. 11, it is found that, the proposed scheme is about 7 to 249 times faster to execute than the MOC scheme, and 34% to 67%

faster than the scheme of Zhao and Ghidaoui.

Test 3: Instantaneous downstream valve closure in a frictionless horizontal pipe (two-phase flow)

This test is used to compare the accuracy and numerical efficiency of the proposed scheme against the fixed-grid MOC scheme for two-phase flows. The two-phase homogeneous mathematical model presented in Martin (1993) is solved when using the MOC scheme. In this case, if shocks are present, the Rankine-Hugoniot conditions are enforced across the shock. The test rig is the same as test 1, except that the fluid is an air-water mixture. The void ratio at the reference pressure (101325 Pa) is assumed to be 0.002 (0.2%). The instantaneous closure of the downstream valve results in the appearance of a shock wave at the downstream end of the pipe. This wave propagates upstream until on reflection against the left boundary, it becomes a rarefaction wave. Fig. 12 shows the pressure profiles at 140 s computed using the MOC scheme and the proposed approach assuming isothermal conditions ($\beta = 1.0$) for two different number of grids. The "Near exact" profile is also presented in this figure. In this test case, all the simulations were carried out using a maximum Courant number of 0.95 to avoid numerical instability problems. It should be noted that in two phase flows, the air content and pressure wave celerity are continuously changing (Eqs. 4 and 5). When using an explicit scheme (as used here) for simulating these flows, it is possible to exceed $Cr = 1.0$ if a Cr close to 1.0 is specified at the beginning of the time step. As shown in Fig. 12, for the same number of grids and maximum Courant number, the timing and magnitude of the shock wave simulated by the proposed scheme is in better agreement with the "Near exact" solution than the MOC scheme.

Fig. 13 displays the simulated pressure traces at the middle of the pipe for two dif-

ferent number of grids. As can be observed in this figure, the MOC is more dissipative than the proposed scheme. The results presented in Figs. 12 and 13 show that, for the same discretization, the proposed scheme is more accurate than the MOC scheme. A more conclusive comparison requires measurement of the CPU time needed by each scheme to achieve a given level of accuracy. The accuracy of a scheme can be measured using the following error norm (e.g., Liang et al. 2007):

$$\text{ABSERROR} = \frac{\Sigma_{i=1}^{Nx} |e_i|}{\Sigma_{i=1}^{Nx} |\phi_i^{\text{exact}}|} \tag{32}$$

where $e_i = \phi_i^{\text{numerical}} - \phi_i^{\text{exact}} =$ difference between the numerical and exact solution at node i, ϕ = dependent variable such as the pressure head or flow velocity, ABSERROR = absolute error, and $Nx =$ number of grids. The absolute error is a measure of the difference between the numerical and exact solution for either the pressure head or flow velocity.

Fig. 14 shows the plot of the absolute error for the pressure head against the number of grids on log-log scale. As shown in this figure, to achieve a given level of accuracy, the MOC scheme requires a finer grid than the proposed scheme, or, for the same number of grids, the proposed scheme is more accurate than the MOC scheme. For comparison of CPU times, four levels of absolute error were selected (0.4% - 10%). The number of grids needed by each of the schemes to achieve the four absolute error levels, were obtained from Fig. 14. These number of grids in turn were used to compute the CPU times, which results are shown in Fig. 15. The CPU time results show that the proposed scheme is about 3 to 130 times faster to execute than the MOC scheme. The numerical efficiency of the proposed scheme compared to the MOC approach increases as the absolute error decreases.

Test 4: Comparison with two-phase flow experiments of Chaudhry et al. (1990)

In this test, the fixed-grid MOC and the proposed scheme are used to reproduce the second set of experiments reported in Chaudhry et al. (1990). The writers are indebted to one of the authors of this paper, namely Professor C. Samuel Martin, who kindly provided us the data for this set of experiments. The schematic of the test facility is shown in Fig. 16. The conditions for the second set of experiments reported in Chaudhry et al. (1990) are presented in Table 1.

The test procedure was as follows: A steady state flow of an air-water mixture was established in the test pipe by controlling the exit valves and the pressure of the injected air at the inlet. The flow velocity of the air-water mixture was maintained at a high enough rate so that slug flow could be avoided by limiting the rate of air injection. Transient flow was created by a rapid valve closure at the downstream end of the pipe. Transient-state pressures were monitored by high-frequency-response pressure transducers at three locations (1, 2 and 3), as shown in Fig. 16. The three stations were located at x = 8 m, 21.1 m and 30.6 m, respectively, from the upstream end.

The upstream boundary was a constant-level reservoir while the downstream boundary was the recorded pressure history at station 3 (x = 30.6 m). A flow discharge boundary condition was not used at the downstream end because the rate of closure of the exit valve was not reported in Chaudhry et al. (1990). They suggested instead to use the recorded pressure history at station 3 as downstream boundary condition because the measurement of the rate of closure of a valve and, consequently the measurement of velocity are very difficult. The recorded pressure trace at station 3 is shown in Fig. 17.

The simulated pressure traces at stations 1 and 2, assuming isothermal (β = 1.0) and

adiabatic (β = 1.4) conditions, are presented with the corresponding experimental observations in Figs. 18 - 21. As shown in these figures, the simulated pressure traces using the MOC and the proposed scheme are very similar for isothermal and adiabatic conditions. Figs. 18 - 21 also show that the simulated peak pressures (MOC and proposed) are higher than those in the experiments for both conditions. In addition, the results show that the simulated pressure traces agree with the experiments better when isothermal conditions (Figs. 18 - 19) were assumed than when adiabatic conditions (Figs. 20 - 21) were assumed. As an aside, a transient phenomena takes place in isothermal conditions when there is no change of temperature during the transient. Likewise, a transient phenomena develops in adiabatic conditions when no heat enters or leaves the system during the transient. In the experiments reported in Chaudhry et al. (1990), neither isothermal nor adiabatic conditions seem to have prevailed. This is believed because the time scale seems too fast for isothermal conditions to prevail. Also, the conductivity of a stainless steel pipe, which is the material of the pipe used in the experiments, is not very low for adiabatic conditions to hold.

Since the thermodynamic conditions during the experiments reported in Chaudhry et al. (1990) were neither isothermal nor adiabatic, several values of β between 1.0 and 1.4 were tested to find the value of β that produces the best fit with the experimental data. This value is found to be 1.05. The simulated pressure traces at stations 1 and 2 using β = 1.05 are presented with the corresponding experimental observations in Figs. 22 and 23, respectively.

By comparing the simulated results achieved by the MOC and the proposed scheme for β = 1.05, it can be seen that the pressure traces computed using the MOC are lower

than the proposed scheme. This means that the MOC is more dissipative than the proposed scheme. However, the MOC agrees with the experiments slightly better than the proposed scheme. This may be confusing because one can conclude that the MOC is more accurate than the proposed scheme. The apparent advantage of the MOC over the proposed scheme is because, as usually is the case, the physical dissipation can not be estimated with good accuracy and it is often underestimated. The last is especially true when the physical dissipation is estimated using only a steady friction formulation (as used here). Even though there are formulations to estimate unsteady friction (e.g., Pezzinga 2000), the physical dissipation often cannot be determined with good accuracy, especially in complex flows such as two-phase flows. As suggested by Cannizzaro and Pezzinga (2005), in two-phase flows, the physical dissipation is not only associated to the wall shear stress but also to thermodynamic processes (e.g., thermic exchange between the gaseous phase and the surrounding liquid and gas release). In general, it is very difficult and it may be misleading to compare the accuracy of numerical schemes using experiments. The discrepancies between simulated and observed values may be attributed to experimental uncertainty and to neglecting unsteady friction and thermodynamic processes when computing the physical dissipation.

Conclusions

This paper focuses on the formulation and assessment of a FV second-order accurate shock-capturing scheme for modeling one and two-phase water hammer flows. The two-phase flow model is based on the single-equivalent fluid concept. The accuracy and efficiency of the proposed scheme is contrasted against the fixed-grid MOC scheme and another FV scheme for one-phase flows, and the fixed-grid MOC scheme for two-phase flows. The fixed-grid MOC and the proposed scheme are also used to reproduce a set of two-phase

flow experiments reported in the literature. For a realistic assessment of the accuracy and numerical efficiency of the schemes in one-phase flow conditions, a variation of the Courant number with the number of grids is introduced. This is important because in pipe systems for one-phase flows, by increasing the number of cells, the average trend of the Courant number in all the pipes increases and approaches 1.0. The key results are as follows:

(1) The results for one-phase flows (pure liquid) show that, when a Courant number (Cr) very close to 1.0 (around 0.99 or higher) is used, the MOC scheme is more efficient than the proposed scheme and the other FV scheme. In this case, the latter two schemes have similar numerical efficiency. When Cr drops below about 0.95, the proposed scheme is more efficient than the MOC scheme and the other FV scheme, especially for smooth transient flows (no discontinuities).

(2) The results for two-phase flows show that the proposed scheme is much more efficient than the fixed-grid MOC scheme. For two-phase water hammer flows, all the simulations were carried out using a maximum Courant number of 0.95 to avoid numerical instability problems.

(3) Good agreement between simulated results using the MOC and the proposed scheme and the two-phase flow experiments is found.

Acknowledgments

The authors gratefully acknowledge Dr. C. Samuel Martin for providing us his two-phase flow experimental data and Dr. Ming Zhao for providing us his one-phase FV and MOC codes. The first, third, and fourth authors wish to thank the financial support of the Metropolitan Water Reclamation District of Greater Chicago (Research Project Specifi-

cation RPS-03). The second author wishes to thank the Research Grant Council of Hong Kong Grant No. HKUST6113/03E.

Appendix A

In this appendix, the Riemann solution for the linearized hyperbolic system $\partial \mathbf{U}/\partial t + \overline{\mathbf{A}}\partial \mathbf{U}/\partial x = 0$ with $\overline{\mathbf{A}} = \mathbf{A}(\overline{\mathbf{U}})$ and $\overline{\mathbf{U}} \equiv (\mathbf{U}_L + \mathbf{U}_R)/2$ will be derived. The two eigenvalues for the matrix $\overline{\mathbf{A}}$ are given by: $\overline{\lambda}_1 = \overline{u} - \overline{a}_m$ and $\overline{\lambda}_2 = \overline{u} + \overline{a}_m$. The application of the Rankine-Hugoniot condition across the two waves [$\overline{\lambda}_i$ $(i = 1,2)$] gives:

$$Qm_\star - Qm_L = (\bar{u} - \bar{a}_m)\big(\Omega_\star - \Omega_L\big) \tag{33}$$

$$Qm_R - Qm_\star = (\bar{u} + \bar{a}_m)\big(\Omega_R - \Omega_\star\big) \tag{34}$$

From Equations 33 and 34 the following relations for $\Omega_\star$ and $Qm_\star$ are obtained.

$$\Omega_\star = \big(\frac{\Omega_L + \Omega_R}{2}\big)\big(1 + \frac{u_L - u_R}{2\bar{a}_m}\big) \tag{35}$$

$$Qm_\star = Qm_L + (\bar{u} - \bar{a}_m)\big(\Omega_\star - \Omega_L\big) \tag{36}$$

Notation

The following symbols are used in this paper:

A = Jacobian matrix of flux vector;

a = pressure-wave celerity in presence of liquid only;

A_f = full cross-sectional area of the conduit;

a_g = general notation for pressure-wave celerity;

a_m = pressure-wave celerity for the gas-liquid mixture;

c_1, c_2 = constants;

Cr = Courant number;

Cr_{max} = maximum Courant number;

d = pipe diameter;

E = total energy;

e_i = difference between the numerical and exact solution at node i;

E_0 = initial total energy;

$\mathbf{F}$ = Flux vector;

f = Darcy-Weisbach friction factor;

$\mathbf{F}^n_{i-1/2}$, $\mathbf{F}^n_{i+1/2}$ = intercell flux;

g = acceleration due to gravity;

H = absolute pressure head in meters of water;

h = piezometric head measured over the conduit bottom;

h_0 = reservoir head measured over the conduit bottom;

k_f = bulk modulus of elasticity of the fluid;

L = length of pipe;

Nx = Number of grids;

p = pressure acting on the center of gravity of A_f;

Q = flow discharge;

Q_m = mass flow discharge;

$\mathbf{S}$ = vector containing source terms;

S_f = friction slope;

S_0 = bed slope;

t = time;

$\mathbf{U}$ = vector of flow variables;

$\widetilde{\mathbf{U}}$ = evolution of $\mathbf{U}$ by half time step using extrapolated values;

u = water velocity;

x = longitudinal coordinate;

Y = Young's modulus of elasticity;

z = elevation;

β = coefficient equal to 1.0 for isothermal processes and 1.4 for adiabatic conditions;

χ = non-dimensional parameter;

Δi = vector difference;

Δt = time step;

Δx = spatial mesh size;

λ = eigenvalues;

Ω = mass of fluid per unit length of conduit;

ϕ = dependent variable such as the pressure head or flow velocity;

ψ = volume fraction of gas

ρ_f = fluid density;

Superscripts

CFL = Courant-Friedrichs-Lewy criterion;

max = maximum;

n = computational time level;

Subscripts

b = boundary;

i = mesh point location in x direction;

L = left state;

R = right state;

ref = reference;

$\star$ = star region;

References

1. Cannizzaro, D., and Pezzinga, G. (2005). "Energy dissipation in transient gaseous cavitation." *J. Hydraul. Eng.*, 131(8), 724-732.
2. Chaudhry, M. H., and Hussaini, M. Y. (1985). "Second-order accurate explicit finite-difference schemes for water hammer analysis." *J. Fluids Eng.*, 107, 523-529.
3. Chaudhry, M. H. (1987). *Applied hydraulic transients*, 2nd edition, Van Nostrand Reinhold, New York.
4. Chaudhry, M. H., Bhallamudi, S. M., Martin, C. S., and Naghash, M. (1990). "Analysis of transient in bubbly homogeneous, gas-liquid mixtures." *J. Fluids Eng.*, 112, 225-231.
5. Ghidaoui, M. S., and Karney, B. W. (1994). "Equivalent differential equations in fixed-grid characteristics method." *J. Hydraul. Eng.*, 120(10), 1159-1175.
6. Ghidaoui, M. S., Karney, B. W., and McInnis, D. A. (1998). "Energy estimates for discretization errors in water hammer problems." *J. Hydraul. Eng.*, 124(4), 384-393.
7. Ghidaoui, M. S., Zhao M., McInnis, D. A., and Axworthy, D. H. (2005). "A review of water hammer theory and practice." *Applied Mechanics Review, ASME*, 58(1), 49-76.
8. Guinot, V. (2000). "Riemann solvers for water hammer simulations by Godunov method." *Int. J. Numer. Methods Eng.*, 49, 851-870.
9. Guinot, V. (2001a). "Numerical simulation of two-phase flow in pipes using Godunov

method." *Int. J. Numer. Meth. in Eng.*, 50, 1169-1189.

10. Guinot, V. (2001b). "The discontinuous profile method for simulating two-phase flow in pipes using the single component approximation." *Int. J. Numer. Meth. Fluids*, 37, 341-359.

11. Guinot, V. (2003). *Godunov-type schemes*, Elsevier Science B.V., Amsterdam, The Netherlands.

12. Hwang, Y-H., and Chung, N-M. (2002). "A fast Godunov method for the water hammer problem." *Int. J. Numer. Meth. Fluids*, 40, 799-819.

13. Karney, B. W. (1990). "Energy relations in transient closed-conduit flow." *J. Hydraul. Eng.*, 116(10), 1180-1196.

14. Karney, B. W., and Ghidaoui, M. S. (1997). "Flexible discretization algorithm for fixed-grid MOC in pipelines." *J. Hydraul. Eng.*, 123(11), 1004-1011.

15. León A. S., Ghidaoui, M. S., Schmidt, A. R., and García M. H. (2005). "Importance of numerical efficiency for real time control of transient gravity flows in sewers." *Proc., XXXI IAHR Congress*, Seoul, Korea.

16. León A. S., Ghidaoui, M. S., Schmidt, A. R., and García M. H. (2006). "Godunov-type solutions for transient flows in sewers." *J. Hydraul. Eng.*, 132(8), 800-813.

17. LeVeque, R. J. (2002). *Finite volume methods for hyperbolic problems*, Cambridge University Press., Cambridge.

18. Liang, J. H., Ghidaoui, M. S., Deng, J. Q., and Gray, W. G. (2007). "A Boltzmann-based finite volume algorithm for surface water flows on cells of arbitrary shapes." *J. Hydraul. Research*, 45(2), 147-164.

19. Martin, C. S. (1993). "Pressure-wave propagation in two-component flow." *Proc.,*

Computer modeling of free-surf. and press. flows, NATO ASI Series E, Applied Sciences Vol. 274, Pullman, WA, U.S.A., 519-552.

20. Padmanabhan, M., and Martin, C. S. (1978). "Shock-wave formation in flowing bubbly mixtures by steepening of compression waves." *Int. J. Multiphase Flow*, 4, 81-88.

21. Pezzinga, G. (2000). "Evaluation of unsteady flow resistances by quasi-2D or 1D models." *J. Hydraul. Eng.*, 126(10), 778-785.

22. Szymkiewicz, R., and Mitosek, M. (2004). "Analysis of unsteady pipe flow using the modified finite element method." *Commun. in Numer. Meth. in Eng.*, 21(4), 183-199.

23. Toro, E. F. (2001). *Shock-capturing methods for free-surface shallow flows*, Wiley, LTD, Chichester, U.K.

24. Wood, D. J., Lingireddy, S., Boulos, P. F., Karney, B. W., and McPherson, D. L. (2005). "Numerical methods for modeling transient flow in distribution systems." *J. of the American Water Works Association*, 97(7), 104-115.

25. Wylie, E. B., and Streeter, V. L. (1983). *Fluid transients*, FEB Press, Ann Arbor, Michigan.

26. Zielke, W., Perko, H. D., and Keller, A. (1989). "Gas release in transients pipe flow." *Proc., 6th International Conference on Pressure Surges*, BHRA, Cambridge, England, Oct. 4-6, 3-13.

27. Zhao, M., and Ghidaoui M. S. (2004). "Godunov-type solutions for water hammer flows." *J. Hydraul. Eng.*, 130(4), 341-348.

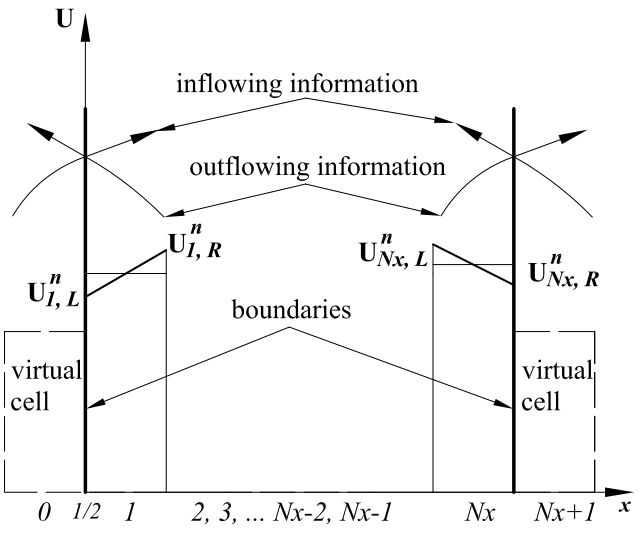

Fig. 1. Second-order boundary conditions by adding virtual cells

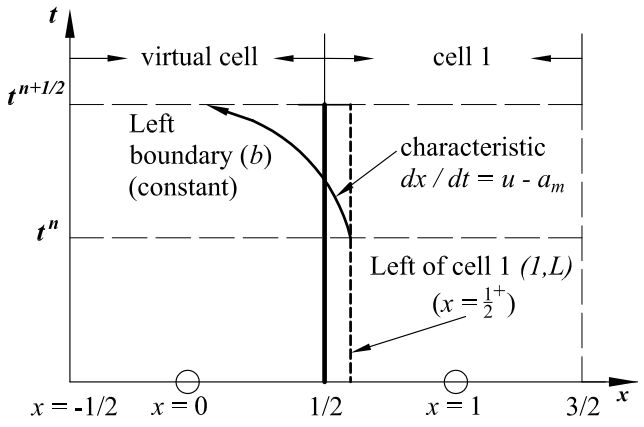

Fig. 2. Path of integration at left-hand boundary

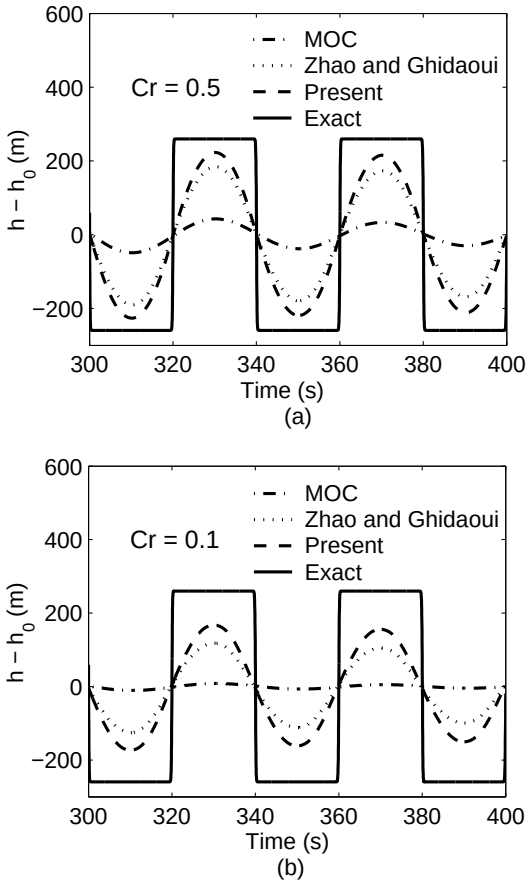

Fig. 3. Pressure traces at downstream valve for test No 1 ($Nx = 10$ cells) using (a) Cr = 0.5, and (b) Cr = 0.1.

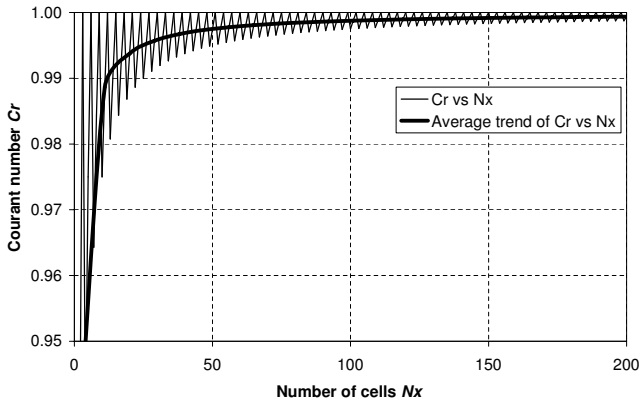

Fig. 4. Courant number versus number of cells

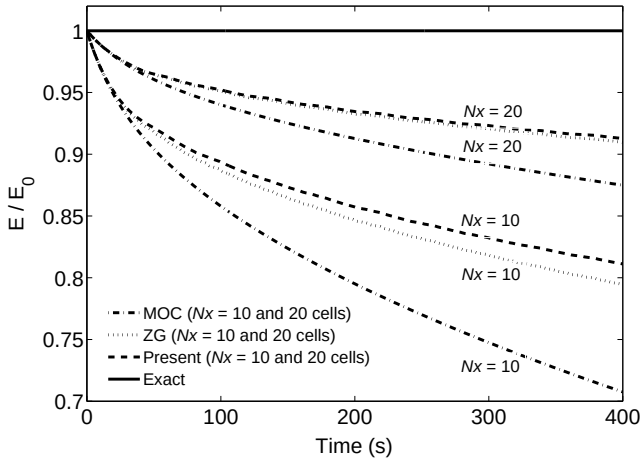

Fig. 5. Energy traces for test No 1 (Nx = 10 cells, Cr = 0.9829; Nx = 20 cells, Cr = 0.9938)

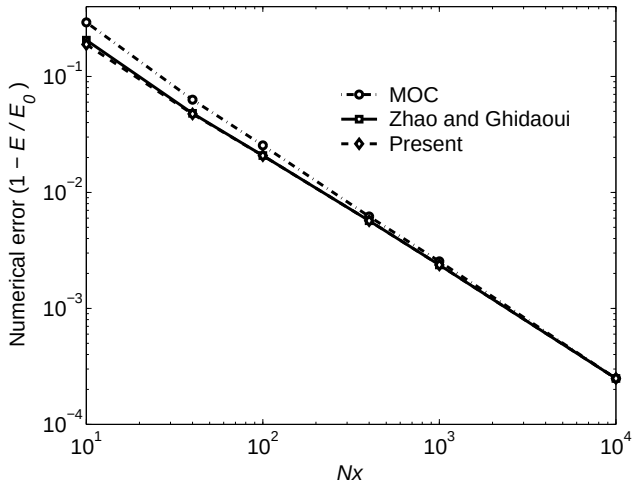

Fig. 6. Numerical error versus number of grids for test No 1 (t = 400 s)

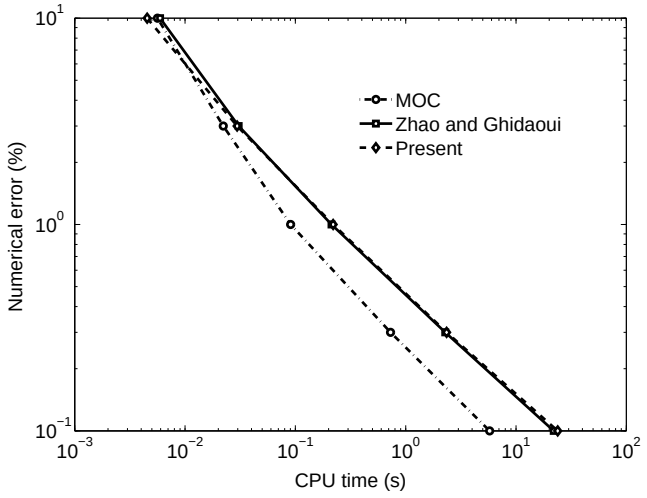

Fig. 7. Relation between level of accuracy and CPU time for test No 1 (t = 400 s)

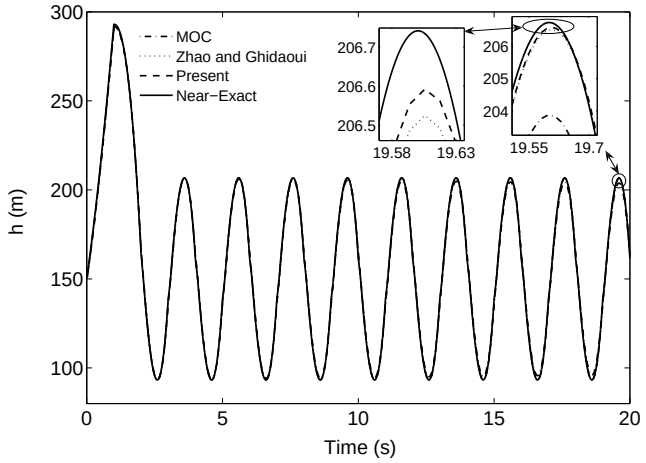

Fig. 8. Pressure traces at downstream valve for test No 2 ($Nx = 40$ cells, $Cr = 0.95$).

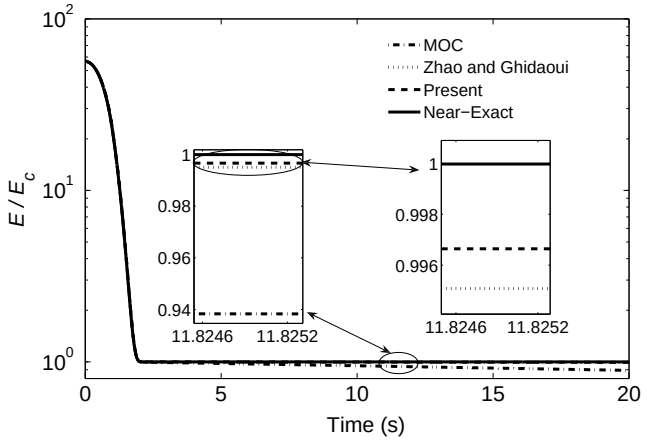

Fig. 9. Energy traces for test No 2 ($Nx = 40$ cells, $Cr = 0.95$).

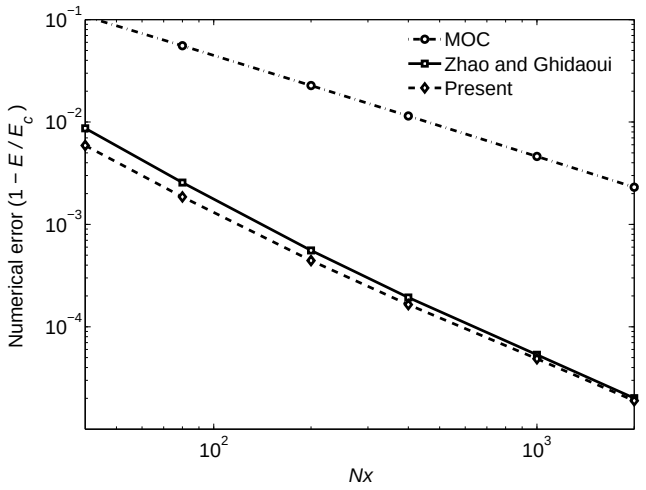

Fig. 10. Numerical error versus number of grids for test No 2 (t = 20 s, Cr = 0.95)

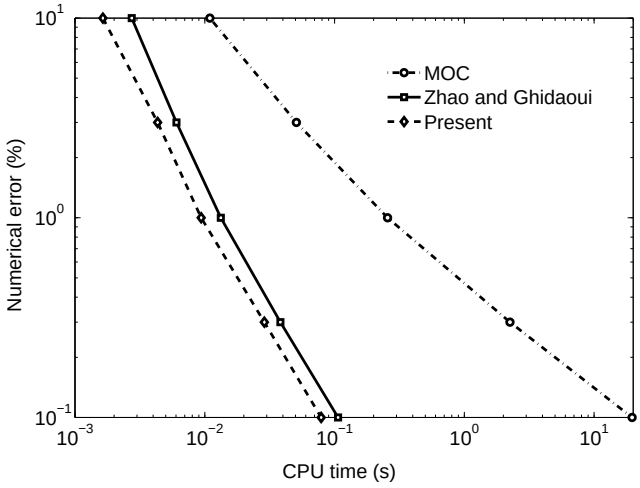

Fig. 11. Relation between level of accuracy and CPU time for test No 2 (t = 20 s, Cr = 0.95)

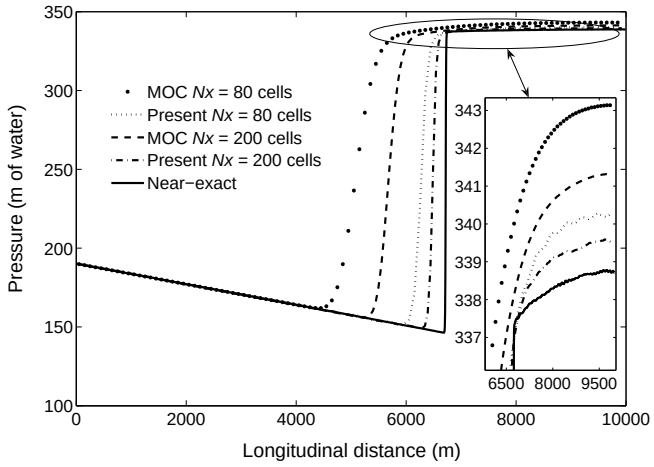

Fig. 12. Pressure head versus longitudinal distance for test No 3 ($\beta = 1$, $t = 140$ s and $Cr_{max} = 0.95$).

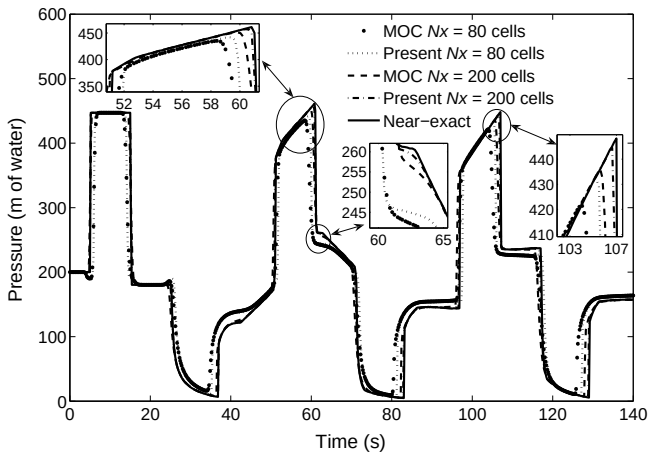

Fig. 13. Pressure traces at the middle of the pipe for test No 3 (β = 1 and Cr_{max} = 0.95).

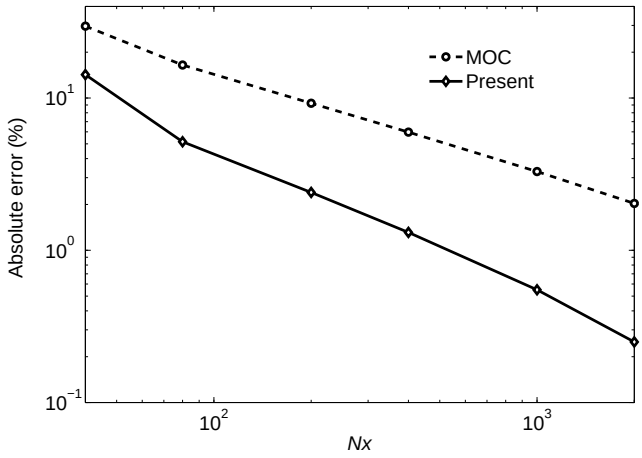

Fig. 14. Absolute error for the pressure head versus number of grids for test No 3 (β = 1, t = 140 s and Cr_{max} = 0.95).

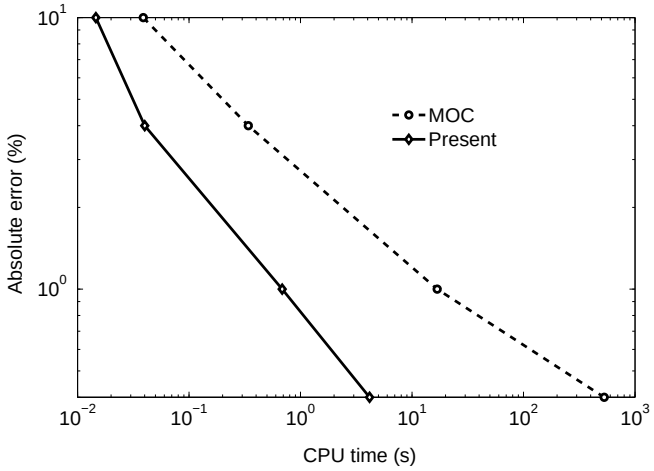

Fig. 15. Absolute error for the pressure head versus CPU time for test No 3 (β = 1, t = 140 s and Cr_{max} = 0.95).

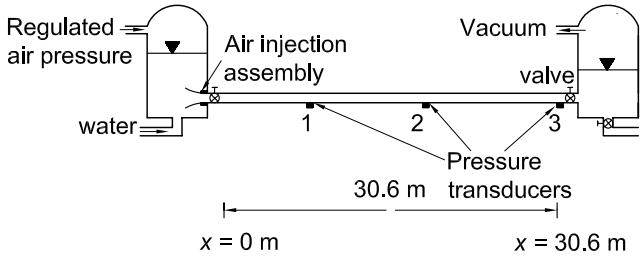

Fig. 16. Schematic of experiment Chaudhry et al. (1990) (schematic used with permission from ASME).

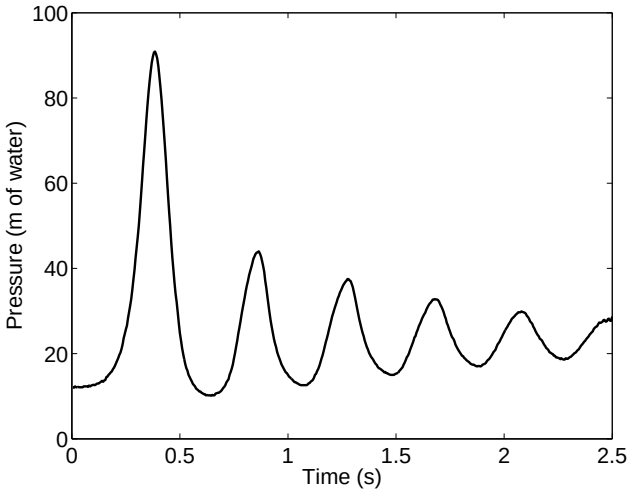

Fig. 17. Experimental absolute pressure trace at downstream end (x = 30.6 m)(experimental data used with permission from ASME).

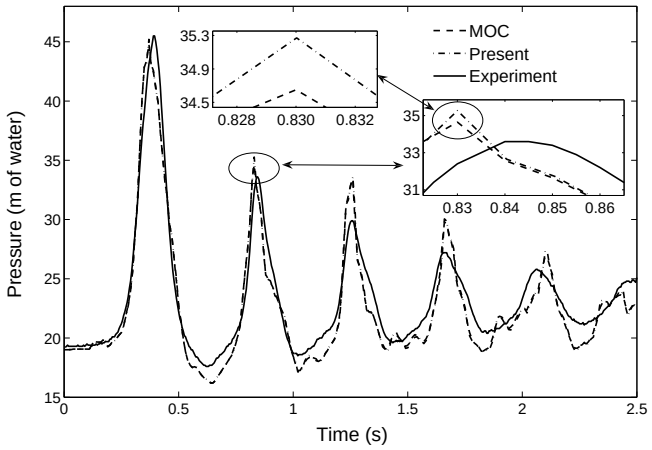

Fig. 18. Computed and experimental absolute pressure traces at $x = 8\ m$ ($Nx = 100$ cells and $Cr_{max} = 0.95$). The computed pressure traces were performed under isothermal conditions ($\beta = 1$)(experimental data used with permission from ASME).

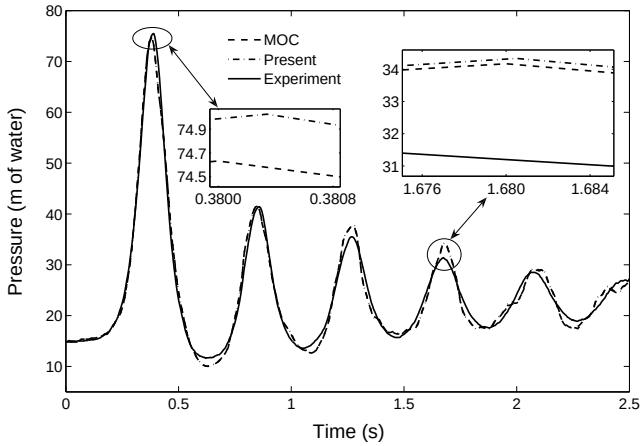

Fig. 19. Computed and experimental absolute pressure traces at x = 21.1 m ($Nx = 100$ cells and Cr_{max} = 0.95). The computed pressure traces were performed under isothermal conditions (β = 1)(experimental data used with permission from ASME).

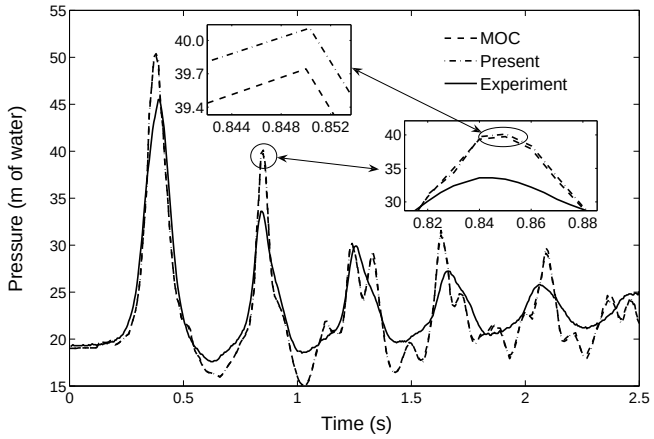

Fig. 20. Computed and experimental absolute pressure traces at x = 8 m ($Nx = 100$ cells and Cr_{max} = 0.95). The computed pressure traces were performed under adiabatic conditions (β = 1.4) (experimental data used with permission from ASME).

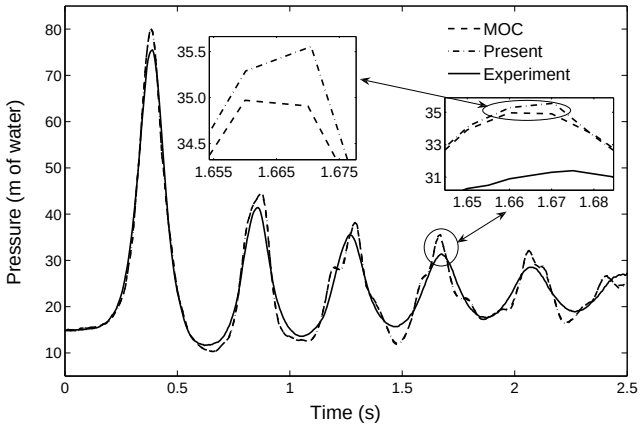

Fig. 21. Computed and experimental absolute pressure traces at x = 21.1 m ($Nx = 100$ cells and Cr_{max} = 0.95). The computed pressure traces were performed under adiabatic conditions (β = 1.4)(experimental data used with permission from ASME).

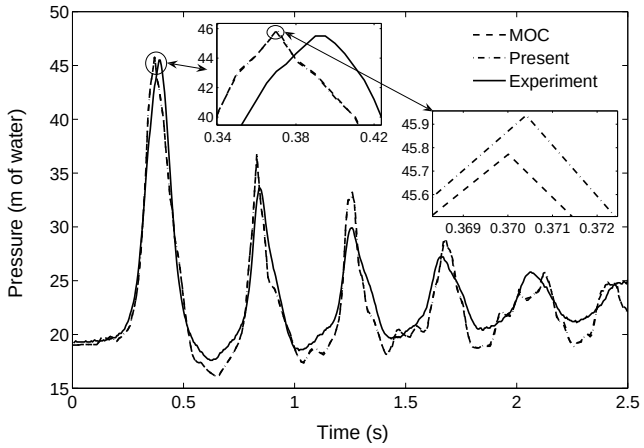

Fig. 22. Computed and experimental absolute pressure traces at x = 8 m (β = 1.05, Nx = 100 cells and Cr_{max} = 0.95)(experimental data used with permission from ASME).

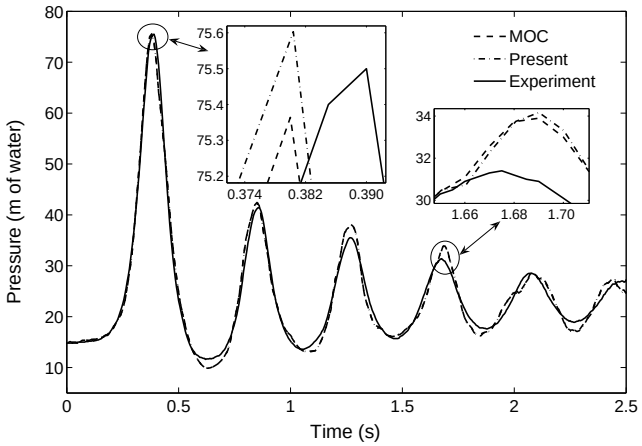

Fig. 23. Computed and experimental absolute pressure traces at x = 21.1 m (β = 1.05, Nx = 100 cells and Cr_{max} = 0.95)(experimental data used with permission from ASME).

Table 1. Experimental conditions for second set of experiments reported in Chaudhry et al. (1990)

Description	**Values**
Length L (m)	30.600
Diameter d (m)	0.026
Bed slope S_0 (m/m)	0.000
Upst. reserv. press. H_0 (m of water absol.)	21.700
Steady flow velocity u_0 (m/s)	2.940
Darcy-Weisbach friction factor f_q	0.0195
Pressure-wave celerity a (m/s)	715.000
Steady air mass flow rate (kg/s)	$1.15\text{x}10^{-5}$
Downstream void ratio ψ_{ref}	0.0053

List of Figure captions

(1) Fig. 1. Second-order boundary conditions by adding virtual cells.

(2) Fig. 2. Path of integration at left-hand boundary.

(3) Fig. 3. Pressure traces at downstream valve for test No 1 ($Nx = 10$ cells) using (a) $Cr = 0.5$, and (b) $Cr = 0.1$.

(4) Fig. 4. Courant number versus number of cells.

(5) Fig. 5. Energy traces for test No 1 ($Nx = 10$ cells, $Cr = 0.9829$; $Nx = 20$ cells, $Cr = 0.9938$).

(6) Fig. 6. Numerical error versus number of grids for test No 1 ($t = 400$ s)

(7) Fig. 7. Relation between level of accuracy and CPU time for test No 1 ($t = 400$ s).

(8) Fig. 8. Pressure traces at downstream valve for test No 2 ($Nx = 40$ cells, $Cr = 0.95$).

(9) Fig. 9. Energy traces for test No 2 ($Nx = 40$ cells, $Cr = 0.95$).

(10) Fig. 10. Numerical error versus number of grids for test No 2 ($t = 20$ s, $Cr = 0.95$).

(11) Fig. 11. Relation between level of accuracy and CPU time for test No 2 ($t = 20$ s, $Cr = 0.95$).

(12) Fig. 12. Pressure head versus longitudinal distance for test No 3 ($\beta = 1$, $t = 140$ s and $Cr_{max} = 0.95$).

(13) Fig. 13. Pressure traces at the middle of the pipe for test No 3 ($\beta = 1$ and $Cr_{max} = 0.95$).

(14) Fig. 14. Absolute error for the pressure head versus number of grids for test No 3 ($\beta = 1$, $t = 140$ s and $Cr_{max} = 0.95$).

(15) Fig. 15. Absolute error for the pressure head versus CPU time for test No 3 ($\beta = 1$, $t = 140$ s and $Cr_{max} = 0.95$).

(16) Fig. 16. Schematic of experiment Chaudhry et al. (1990) (schematic used with permission from ASME).

(17) Fig. 17. Experimental absolute pressure trace at downstream end (x = 30.6 m)(experimental data used with permission from ASME).

(18) Fig. 18. Computed and experimental absolute pressure traces at x = 8 m ($Nx =$ 100 cells and Cr_{max} = 0.95). The computed pressure traces were performed under isothermal conditions (β = 1)(experimental data used with permission from ASME).

(19) Fig. 19. Computed and experimental absolute pressure traces at x = 21.1 m ($Nx =$ 100 cells and Cr_{max} = 0.95). The computed pressure traces were performed under isothermal conditions (β = 1)(experimental data used with permission from ASME).

(20) Fig. 20. Computed and experimental absolute pressure traces at x = 8 m ($Nx = 100$ cells and Cr_{max} = 0.95). The computed pressure traces were performed under adiabatic conditions (β = 1.4) (experimental data used with permission from ASME).

(21) Fig. 21. Computed and experimental absolute pressure traces at x = 21.1 m ($Nx = 100$ cells and Cr_{max} = 0.95). The computed pressure traces were performed under adiabatic conditions (β = 1.4)(experimental data used with permission from ASME).

(22) Fig. 22. Computed and experimental absolute pressure traces at x = 8 m (β = 1.05, $Nx = 100$ cells and Cr_{max} = 0.95)(experimental data used with permission from ASME).

(23) Fig. 23. Computed and experimental absolute pressure traces at x = 21.1 m (β = 1.05, $Nx = 100$ cells and Cr_{max} = 0.95)(experimental data used with permission from ASME).